Physica B 452 (2014) 119–123

Contents lists available at ScienceDirect

Physica B

journal homepage: www.elsevier.com/locate/physb

Electronic structure of CdTe using GGA+U^{SIC}

E. Menéndez-Proupin [a,b,*], A. Amézaga [a,c], N. Cruz Hernández [d]

[a] Departamento de Física, Facultad de Ciencias, Universidad de Chile, Las Palmeras 3425, 780-0003 Ñuñoa, Santiago, Chile
[b] Instituto de Energía Solar and Dept. Tecnologías Especiales, E.T.S.I. Telecomunicación, Universidad Politécnica de Madrid, Spain
[c] Instituto de Ciencias Físicas y Matemáticas, Universidad Austral de Chile, Casilla 567, Valdivia, Chile
[d] Departamento de Física Aplicada I, Escuela Técnica Superior de Ingeniería Informática, Universidad de Sevilla, Av. Reina Mercedes, 41012 Sevilla, Spain

ARTICLE INFO

Article history:
Received 3 May 2014
Received in revised form
5 July 2014
Accepted 8 July 2014
Available online 15 July 2014

Keywords:
Electronic structure
Gap correction
Cadmium telluride

ABSTRACT

A simple method to obtain a gap-corrected band structure of cadmium telluride within density functional theory is presented. On-site Coulomb self-interaction-like correction potential has been applied to the 5p-shell of Te and the 4d-shell of Cd. The predicted physical properties are similar to or better than those obtained with hybrid functionals and at largely reduced computational cost. In addition to the corrected electronic structure, the lattice parameters and the bulk modulus are improved. The relative stabilities of the different phases (zincblende, wurtzite, rocksalt and cinnabar) are preserved. The formation energy of the cadmium vacancy remains close to the values obtained from hybrid functional calculations.

1. Introduction

Cadmium telluride is a semiconductor material with a long history of applications, such as radiation detectors and photovoltaic devices. In particular, CdTe thin-film solar cells have been greatly improved during the last decade and are challenging the silicon solar market. CdTe presents crystalline structure and electronic properties common to traditional inorganic semiconductors. Therefore, its electronic properties are well understood. In particular, its band diagram was determined by Chelikowsky and Cohen many years ago [1,2], by means of empirical pseudopotential calculations with parameters fitted to experimental data.

The CdTe photovoltaic response is greatly modulated by the thermodynamic and electronic properties of defects, impurities and grain boundaries, which are much more difficult to characterize than the pure material. In fact, in many situations the identification of the defects and impurities is uncertain, and theoretical calculations have provided insights into their nature and the doping limits [3]. Complementary to experimental techniques, density functional theory (DFT) constitutes a powerful theoretical tool for calculating quantum electronic states of atoms, molecules, and extended solids. The main virtue of DFT is that it is a predictive method, free of system-dependent parameters, and has been extremely successful in the calculation of ground state electronic properties. To a lesser extent, DFT is an invaluable tool for a first estimation of excited state properties. A famous and controversial problem of practical DFT approximations, such as local density approximation (LDA) and generalized gradient approximation (GGA), is the underestimation of the valence–conduction band gaps. For inorganic semiconductors like CdTe, the DFT band gaps are typically 50% of the experimental gaps. Gap underestimation is severe in CdTe: the gap is estimated at approximately 0.3 eV when the spin–orbit coupling is included in the calculation, compared with 1.6 eV experimental value [1,2]. Disregarding the conceptual difference between the DFT and the experimental band gap, the failure to reproduce the gaps affects the predictive capability of certain ground-state calculations. One example is the calculation of thermodynamical properties of donor impurities, where empirical gap corrections are applied to total energies given by LDA and GGA calculations [4,5]. Moreover, deep in-gap defect levels and their total energies, which are not perturbed states of a single (conduction or valence) band, cannot be obtained from single corrections to LDA/GGA calculations [3,5]. Hybrid functionals [6,7] that include a fraction of Hartree–Fock exchange, and the quasiparticle Green function formalism GW [8,9], enable the electronic structure to be attained in generally better agreement with experiments. However, the computational cost is increased by one or two orders of magnitude, and this constitutes a severe limitation for supercells containing nearly 100 atoms. Therefore, it is convenient to explore alternative methods that tackle particular scientific problems at reduced computational cost and are, at the same time, self-consistent and adaptable to various chemical environments. Two examples are the addition of empirical nonlocal external potentials (independent of the electron state) and the inclusion of empirical electron–electron

* Corresponding author at: Departamento de Física, Facultad de Ciencias, Universidad de Chile, Las Palmeras 3425, 780-0003 Ñuñoa, Santiago, Chile. Tel.: +56 2 2978 7439; fax: +56 2 2271 2973.
E-mail address: emenendez@uchile.cl (E. Menéndez-Proupin).

http://dx.doi.org/10.1016/j.physb.2014.07.015
0921-4526/

interaction terms, the strength of which can be fitted to the gap or other electronic properties [5]. The latter approach is followed in this paper.

In the case of CdTe, as in other II–VI compounds, the band gap underestimation is related to the underestimation in LDA/GGA of the binding energy of semicore Cd 4d levels. Therefore, the Cd 4d and Te 5p levels present an incorrectly large hybridization that pushes upwards the top valence band composed mainly of Te 5p levels [10]. LDA and GGA predict the Cd 4d electron bands to occur about 3 eV higher than the experimental band observed in X-ray photoelectron spectra [11,12]. This defect in the calculated binding energy of the cation d-band is common in II–VI compounds, and it has not been resolved completely, even using expensive self-consistent GW methods [13,14].

The origin of the binding energy underestimation is the self-interaction error that, in LDA/GGA, exerts a greater effect on the more localized levels. The on-site Coulomb interaction correction to LDA (LDA+U) and GGA (GGA+U) adds a penalty function to the total energy, and depends on the repulsion and exchange Coulomb integrals, U and J, respectively. In a simplified approach [15], the penalty function is proportional to a single parameter $U' = U - J$ per atomic subshell [15]:

$$\Delta E = \frac{U'}{2}\sum_{\sigma}\left[\sum_{m} n^{\sigma}_{m,m} - \sum_{m,m'} n^{\sigma}_{m,m'} n^{\sigma}_{m',m}\right] \quad (1)$$

where $n^{\sigma}_{m,m'}$ is the density matrix of electrons at each atomic subshell of spin σ. In calculations with spin–orbit coupling, σ is not a valid quantum number and the density matrices are twice as large as those in standard calculations. It this formulation, the double counting correction is the negative of the second term in Eq. (1) [15].

Positive values $U' > 0$ are appropriate for localized states such as Cd 4d subshell, increasing the electron–electron repulsion and enlarging the exchange-correlation hole. With the appropriate U'_d parameter, the binding energy of the Cd 4d band can be fitted, solving the problem of the hybridization with the Te 5p band. With this correction, the band gap values are improved, but not totally. It has been argued that negative values $U' < 0$ are appropriate for delocalized anion s and Te p subshells, where the exchange-correlation hole is overestimated by LDA [16]. Indeed, setting negative U'_s [5,17] or U'_p [16] for the anion s and p subshells, the gap can be better corrected and the overall band structure is improved. This method is called GGA+U$^{\mathrm{SIC}}$; SIC means the self-interaction correction [16]. However, the use of U'_s degrades the equilibrium lattice constants [5]. As will be seen here, the use of U'_p improves the lattice constants and the bulk modulus, and constitutes, in principle, a better option.

This paper is organized as follows. The computational methods are explained in Section 2, and the results are discussed in Section 3. Computational costs are compared in Section 4. Section 5 is devoted to our conclusions.

2. Computational details

A plane-wave projector augmented wave [18,19] scheme has been used, as implemented in the Vienna Ab Initio Simulation Package (VASP) [20,21]. The GGA exchange-correlation functional of Perdew, Burke, and Ernzerhof (PBE) [22] has been used for GGA and GGA+U calculations. We have also used the hybrid functional of Heyd, Scuseria and Ernzerhof (HSE) [6,7]. This functional generally allows better band gaps and better structural properties than PBE to be obtained, at the cost of a great increment in computer time.

A plane wave cutoff of 460 eV has been used for the wave functions. The Brillouin zones of all the structures considered were sampled with Γ-centred k-point grids, automatically generated to have a maximum separation $\Delta k = 0.22\ \mathrm{\AA}^{-1}$. With this setting, an $8\times8\times8$ k-point grid is generated for the primitive cell of the zincblende structure, which is used in this work. This setting allows a convergence of 0.5 meV/atom and 0.4 kbar in total energy and pressure, respectively, for the zincblende structure. In fact, a reduced cutoff of 285 eV permits a convergence within 10 meV/atom in total energy, but the properties derived from relative energies, e.g., lattice constants and bulk moduli, remain well converged. The spin–orbit coupling is included self-consistently in the calculations.

3. Results and discussion

3.1. Optimized U parameters

Fig. 1 shows a set of DOS corresponding to different effective on-site parameters U_d and U_p. While the parameter U_d has physically reasonable values, U_p seems to be excessively large in absolute values. There are two possible reasons. First, both Te 5s and Te 5p levels need to be corrected with negative U parameters, but VASP only allows one atomic shell to be corrected for each element. Thus, the U_p indirectly contains the correlation of Te 5s levels, since they are implicitly linked with Te 5p levels through the formal sp^3 hybridization. Second, the onsite correlation parameterized by U_p is projected onto Te 5p atomic orbitals as defined in the PAW implementation, while the valence and conduction bands are the extended states. Despite the apparently unphysical

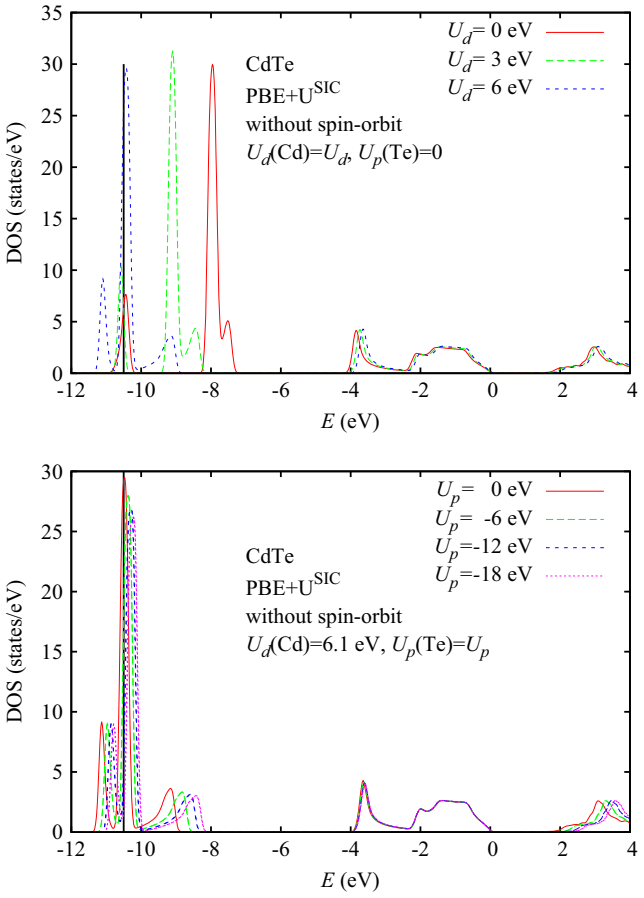

Fig. 1. Density of states of CdTe as a function of the Cd and Te effective parameters U_d(Cd) and U_p(Te), respectively. The spin–orbit coupling is not included in this calculation. The vertical black line at −10.5 eV indicates the experimental binding energy of the Cd 4d band [11].

values of U_p, it is shown below that the band structure and the equation of state are improved with this setting. In Fig. 1, it can be appreciated that U_d strongly modifies the binding energy of the Cd 4d band. Contrary to common belief, the effect of U_d on the valence-conduction gap is rather small (from 0.59 to 0.84 eV, $\Delta E_g/\Delta U_d = 0.042$). The effect of U_p on the gap is somewhat larger, although it tends to saturate ($\Delta E_g/\Delta U_p = -0.060$ for $-6 < U_p < 0$, and $\Delta E_g/\Delta U_p = -0.042$ for $-20 < U_p < 0$). The binding energy of the Cd 4d band is slightly reduced by $U_p < 0$, but this dependence is much weaker than that for U_d. Hence, both physical parameters, the valence–conduction band gap and the Cd 4d band binding energy, can be fitted by the pair of parameters U_d and U_p. Note that this result is contradictory with the attribution of gap underestimation to mixing of Cd 4d and Te 5p states and upwards pushing of the valence band maximum [10]. The aforementioned numbers were computed without the spin–orbit coupling. Spin–orbit coupling splits the valence top band, so that upper bands shift by 0.30 eV, thereby reducing the gap by the same amount. When the spin–orbit coupling is introduced in the calculation, the gap and the Cd 4d binding energy are obtained for $U_d = 5.7$ eV and $U_p = -25.7$ eV. The following results are obtained with this setting.

3.2. Band diagrams

Fig. 2 shows the band diagram computed with three different approximations, PBE, PBE+U^{SIC}, and HSE, each of which includes the spin–orbit coupling. The unit cells have been relaxed to zero pressure for each functional. The experimental band structure is shown as points taken from Ref. [1]. Notice that the Cd 4d bands are not included in the experimental band diagram.

None of the bands agrees completely with the experimental bands. The PBE approximation strongly underestimates the band gap and the energies of all empty bands, although these can be corrected by an almost constant *scissors* shift. The gap is corrected in HSE and PBE+U^{SIC}. HSE underestimates the gap by 0.3 eV, while this is exact in PBE+U^{SIC} due to the fitting procedure. However, the dispersion of the lowest conduction band is slightly weak in PBE+U^{SIC}, while it looks better in HSE.

The spin–orbit splitting of the valence bands at Γ is reproduced correctly by HSE and PBE, and it is underestimated by 0.3 eV by PBE+U^{SIC}. The dispersion of the split-off band (from -4.8 to -0.9 eV) is slightly underestimated in PBE and in PBE+U^{SIC}. The binding energy of the Cd 4d band is underestimated in the PBE framework, as discussed above, and it is fitted in PBE+U^{SIC}. In HSE, it is underestimated by nearly 0.9 eV. For the Te 5s band (~ -10 eV), its position at Γ is correct in PBE, but the dispersion is underestimated. For PBE+U^{SIC}, the band is higher than in the experiment, and the dispersion is fine, while for HSE, the band is lower and the dispersion is underestimated again.

The electrostatic average potential is similar in HSE and PBE+U^{SIC}, 0.2 and 0.3 eV higher than for PBE, respectively. Alternatively, one can state that the valence band maximum (VBM) with respect to the average potential is lower in HSE and PBE+U^{SIC}. This yields beneficial properties, as the same trend is found in GW calculations.

3.3. Equations of state

Let us explore the capability of the PBE+U^{SIC} method for the calculation of the total energy and for the prediction of stable structures. Fig. 3 shows the energy vs volume ($E-V$) curves for the most important crystalline phases: zincblende (ZB), wurtzite (WZ), rocksalt (RS) and cinnabar (CN). The WZ phase is never observed in CdTe, but its possibility must be considered due to its close energy values, and its frequent observation in other II–VI

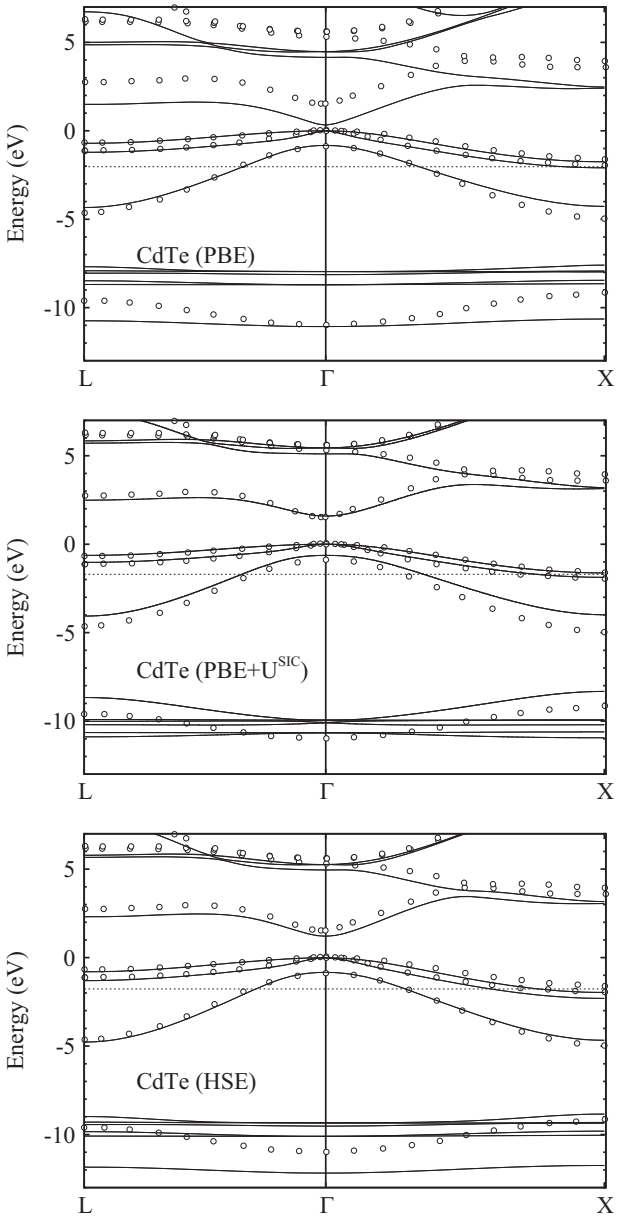

Fig. 2. CdTe bands computed with the functionals PBE, PBE+U^{SIC}, and HSE, compared with the reference data (open circles) [1]. The dotted line indicates the average electrostatic potential.

compounds. The three methods, PBE, HSE and PBE+U^{SIC}, predict that ZB has the lowest energy at low pressures, and the energy of WZ is slightly greater than that of ZB for all volumes. Moreover, the experimental lattice constant and bulk modulus given by PBE+U^{SIC} match better the experimental values, $V_0 = 68.06$ Å^3, $B_0 = 44.5$ GPa [23].

The agreement for high pressure phases, rocksalt (RS) and cinnabar (CN), is somewhat less satisfactory. For both PBE and PBE+U^{SIC}, when the volume decreases, CN transforms into RS, which can be seen in Fig. 3 as the kinks at 52–53 Å^3. In experiments [24], a transition is observed from ZB into a mixture ZB–CN when pressure increases over 34 kbar, and into RS at 38 kbar. On decreasing the pressure, a single-phase CN is observed between 36 and 27 kbar. The experimental differences on increasing and decreasing the pressure suggest various transition paths, the investigation of which lies beyond the scope of this work. Our calculations do not reproduce the stability of the CN phase at any

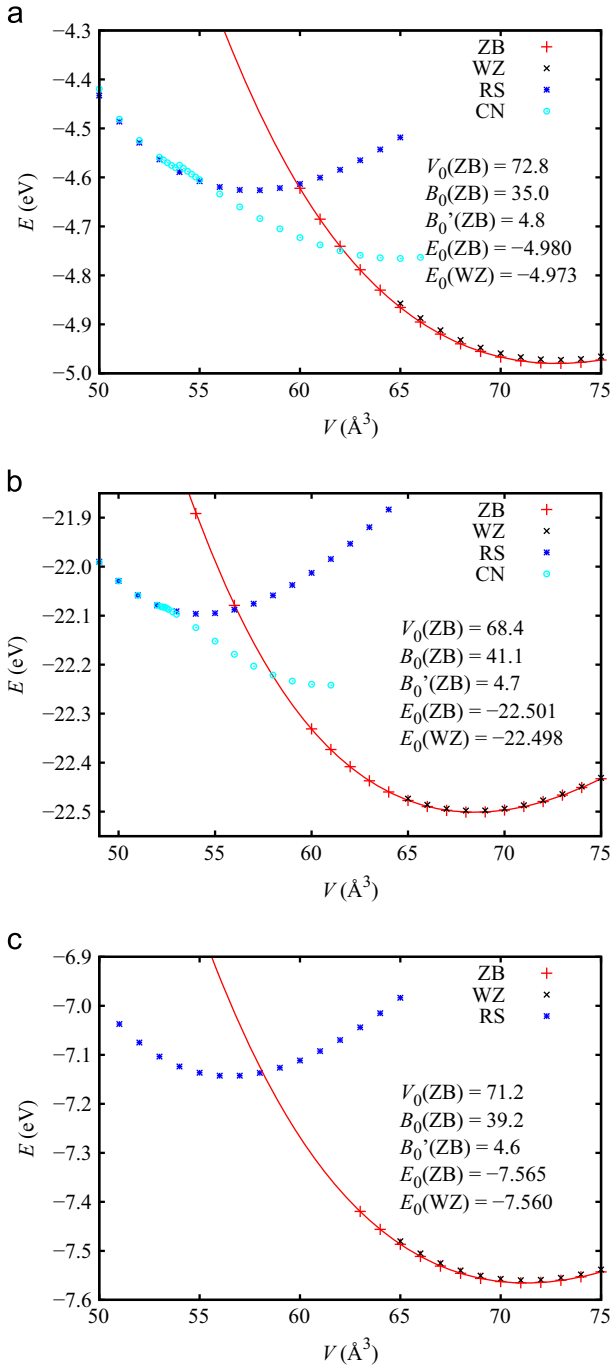

Fig. 3. Energy per CdTe formula unit vs volume for various phases: zincblende (ZB), wurtzite (WZ), rocksalt (RS) and cinnabar (CN).

pressure, they only predict transition from ZB to RS at 40 kbar (PBE) or 51 kbar (PBE+U^{SIC}). With the HSE functional, we have not been able to obtain the CN equation of state, but the transition ZB into RS has been found at 50 kbar, in agreement with PBE+U^{SIC}. The same failure to reproduce the ZB to RS transition has been found using the LDA [25], and it has been shown to depend on tiny errors in the total energy.

3.4. Vacancy formation energy

As a final application, we have calculated the formation energies of the cadmium vacancy V_{Cd}. Following Refs. [4,5], the

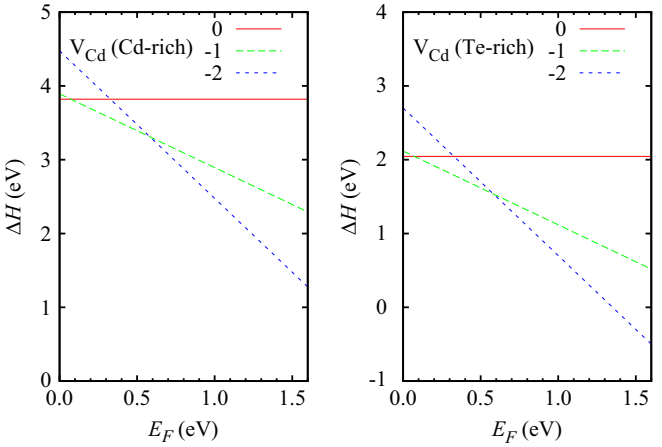

Fig. 4. Formation energy of the cadmium vacancy as a function of the Fermi level, for Cd-rich and Te-rich conditions, and for charge states $q = 0, -1, -2$.

formation energy has been obtained as

$$\Delta H = E(V_{Cd}^q) - E_0 + E(Cd) + \Delta\mu_{Cd} + q(E_{VBM} + E_F) + \Delta E_{size}. \quad (2)$$

Here, E_0 is the energy of a supercell $Cd_{32}Te_{32}$ of the ideal crystal, and $E(V_{Cd}^q)$ is the energy of the same supercell with a Cd vacancy and $-q$ extra electrons (net charge). E(Cd) is the energy per atom of bulk metallic cadmium. The Fermi level E_F is defined with respect to the VBM of the perfect crystal E_{VBM}. Cd-rich and Te-rich conditions are considered as thermodynamical equilibrium with bulk Cd ($\Delta\mu_{Cd} = 0$) and bulk Te ($\Delta\mu_{Cd} = \Delta H$(CdTe)), respectively. ΔH(CdTe) = −1.775 eV is the CdTe formation energy. Size-effect corrections ΔE_{size} include the effects of band filling, image charge, and potential alignment as described in Ref. [5].

The formation energies are shown in Fig. 4, as functions of the Fermi level. The transition levels $\varepsilon(0/-)$ and $\varepsilon(-/-2)$ are 0.07 and 0.58 eV, respectively. For the neutral defect, $\Delta H = 3.82$ eV (Cd-rich) is found, which is higher than the value 3.5 eV obtained using the functional PBE0 (0.165) [26]. It is difficult to assess which value is better due to the lack of experimental values for comparison purposes. On the one hand, the band-filling correction, which is not mentioned in Ref. [26], contributes 0.22 eV in our calculation. On the other hand, the energy differences computed with PBE+U^{SIC} are hampered by the fact that the U parameters are optimized for CdTe, but not necessarily for bulk Cd and Te. HSE calculations may also be biased, since hybrid functionals perform better for insulators than for metals. However, despite small numerical differences, PBE+U^{SIC} and HSE present good overall agreement, and each represents significant corrections to the LDA/GGA results.

4. Computational cost

The cost of the self-consistent field (SCF) calculation of a 64-atom CdTe supercell is compared. The computation time and the number of iterations of the SCF cycle are compared for PBE+U^{SIC} vs the standard PBE and the hybrid HSE, using the spin–orbit interaction in all cases. All the calculations were performed using 64 parallel processes running on POWER7 architecture. Two algorithms for the electronic energy minimization have been tested: the blocked-Davidson and the damped-dynamics algorithms [21]. HSE calculations cannot use the blocked-Davidson algorithm and must be carried out with the slower damped-dynamics algorithm. In Table 1, it can be seen that PBE+U^{SIC} calculations need more SCF iterations than does PBE to converge, and the time per iteration is roughly the same. HSE calculations require a reduced wave function cutoff of 285 eV and a $2 \times 2 \times 2$ k-points mesh,

Table 1
CPU time and number of self-consistent field iterations needed for ground-state calculation of a CdTe 64-atom supercell. Two algorithms for electronic relaxation are compared: Davidson and damped dynamics.

	PBE[a]	PBE+U^{SIC}[a]	HSE[b]
Davidson algorithm			
Time (s)	14 879	27 744	
SCF iterations	22	44	
Damped dynamics algorithm			
Time (s)	48 211	69 248	161 074
SCF iterations	27	34	28

[a] Standard cutoff 460 eV and k-points set $3\times3\times3$.
[b] Reduced cutoff 285 eV and k-points set $2\times2\times2$.

instead of 460 eV and $3\times3\times3$ used for PBE and PBE+U^{SIC}. With the larger cutoff the calculation fails to converge in the 72-h time allowance of the supercomputer. Even with these soft computational parameters, the HSE computation time is significantly larger than with PBE+U^{SIC}.

5. Conclusions

The use of PBE+U^{SIC} for CdTe allows the band structure from self-consistent calculations to be attained, thereby achieving good agreement with the experimental data and the empirical pseudopotential method. Therefore, CdTe adds to the list of semiconductors that have been successfully described by LDA+U^{SIC} [16]. The accuracy of PBE+U^{SIC} is comparable with that of the hybrid functional HSE method, with similar values of the fundamental band gap, the band dispersion, the relative positions of the VBM, and the average potential, and gives better values for the lattice constant and the bulk modulus. The band gap has been used to fit the parameters U_p and U_d, but not the other properties. Naturally, an optimized HSE functional for CdTe could be obtained by refitting the fraction of Hartree–Fock exchange and the screening constant, but this is almost unnecessary as the HSE functional is quite good for CdTe and other semiconductors. The motivation for a fitted PBE+U^{SIC} method is to obtain computational advantages. The computational cost of PBE+U^{SIC} is a fraction of the cost of hybrid functionals, which is crucial for calculation of medium-sized/large systems, such as the models of defects in semiconductors. The present method may be optimized with minor coding efforts, such as allowing on-site corrections to multiple shells per atom, e.g., s and p simultaneously. Other interesting possibility is the recent GGA+U+V method, which includes inter-site electronic interactions to treat covalent compounds [27].

Acknowledgments

This work was supported by FONDECYT Grant nos. 1110602 and 1130437. The authors thankfully acknowledge the computer resources, technical expertise and assistance provided by the Madrid Supercomputing and Visualization Center (CeSViMa) and Red Española de Supercomputación.

References

[1] J.R. Chelikowsky, M.L. Cohen, Phys. Rev. B 14 (1976) 556.
[2] O. Madelung (Ed.), Landolt–Börnstein Numerical Data and Functional Relationships in Science and Technology, vol. III/7b, Springer, Berlin, 1986.
[3] C. Freysoldt, B. Grabowski, T. Hickel, J. Neugebauer, G. Kresse, A. Janotti, C.G. Van de Walle, Rev. Mod. Phys. 114 (2014) 14.
[4] C. Persson, S. Lany, A. Zunger, Phys. Rev. B 72 (2005) 035211.
[5] S. Lany, A. Zunger, Phys. Rev. B 78 (2008) 235104.
[6] J. Heyd, G.E. Scuseria, M. Ernzerhof, J. Chem. Phys. 118 (2003) 8207.
[7] J. Heyd, G.E. Scuseria, M. Ernzerhof, J. Chem. Phys. 124 (2006) 219906.
[8] P. Rinke, A. Qteish, J. Neugebauer, C. Freysoldt, M. Scheffler, New J. Phys. 7 (2005) 126.
[9] A. Fleszar, W. Hanke, Phys. Rev. B 71 (2005) 045207.
[10] S.-H. Wei, A. Zunger, Phys. Rev. B 37 (1988) 8958.
[11] D. Vogel, P. Krüger, J. Pollmann, Phys. Rev. B 54 (1996) 5495.
[12] E. Menéndez-Proupin, G. Gutiérrez, E. Palmero, J.L. Peña, Phys. Rev. B 70 (2004) 035112.
[13] M. Shishkin, G. Kresse, Phys. Rev. B 75 (2007) 235102.
[14] M. Shishkin, M. Marsman, G. Kresse, Phys. Rev. Lett. 99 (2007) 246403.
[15] S.L. Dudarev, G.A. Botton, S.Y. Savrasov, C.J. Humphreys, A.P. Sutton, Phys. Rev. B 57 (1998) 1505.
[16] C. Persson, S. Mirbt, Brazil. J. Phys. 36 (2006) 286.
[17] T.R. Paudel, W.R.L. Lambrecht, Phys. Rev. B 77 (2008) 205202.
[18] P.E. Blöchl, Phys. Rev. B 50 (1994) 17953.
[19] G. Kresse, D. Joubert, Phys. Rev. B 59 (1999) 1758.
[20] G. Kresse, J. Furthmüller, Comput. Mater. Sci. 6 (1996) 15.
[21] G. Kresse, J. Furthmüller, Phys. Rev. B 54 (1996) 11169.
[22] J.P. Perdew, K. Burke, M. Ernzerhof, Phys. Rev. Lett. 77 (1996) 3865.
[23] B.K. Agrawal, S. Agrawal, Phys. Rev. B 45 (1992) 8321.
[24] M.I. McMahon, R.J. Nelmes, N.G. Wright, D.R. Allan, Phys. Rev. B 48 (1993) 16246.
[25] M. Côté, O. Zakharov, A. Rubio, M.L. Cohen, Phys. Rev. B 55 (1997) 13025.
[26] K. Biswas, M.-H. Du, New J. Phys. 14 (2012) 063020.
[27] B. Himmetoglu, A. Floris, S. de Gironcoli, M. Cococcioni, Int. J. Quantum Chem. 114 (2014) 14.